Supramolecular nanostructured assemblies of different types of porphyrins with fullerene using TiO_2 nanoparticles for light energy conversion

Taku Hasobe,[a,b] Shigeki Hattori,[a] Prashant V. Kamat,[*,b] and Shunichi Fukuzumi[*,a]

Department of Material and Life Science, Graduate School of Engineering, Osaka University, SORST, Japan Science and Technology Agency, Suita, Osaka 565-0871, Japan

Radiation Laboratory and Department of Chemical & Biomolecular Engineering, University of Notre Dame, Notre Dame, Indiana 46556, USA

---

[a] Osaka University, [b] University of Notre Dame

E-mail: fukuzumi@ap.chem.eng.osaka-u.ac.jp, pkamat@nd.edu

Abstract

TiO_2 nanoparticles were modified with porphyrin derivatives, 5-[4-benzoic acid]-10,15,20-tris[3,5-di-*tert*-butylphenyl]-21*H*,23*H*-porphyrin (**Ar-H_2P-COOH**), 5-[4-benzoic acid]-10,20-tris[3,5-di-*tert*-butylphenyl]-21*H*,23*H*-porphyrin (**H-H_2P-COOH**), and 5,10,15,20-tetra[4-benzoic acid]-21*H*,23*H*-porphyrin (**H_2P-4COOH**). The porphyrin-modified TiO_2 nanoparticles were deposited on nanostructured OTE/SnO_2 electrode together with nanoclusters of fullerene (C_{60}) in acetonitrile/toluene (3:1, v/v) using an electrophoretic deposition technique to afford the porphyrin-modified TiO_2 composite electrode denoted as OTE/SnO_2/(porphyrin-modified TiO_2 nanoparticle+C_{60})$_n$. The porphyrin-modified TiO_2 composite electrodes have efficient light absorbing properties in the visible region, exhibiting the photoactive response under visible light excitation using I_3^-/I^- redox couple. The incident photon to photocurrent efficiency (IPCE) values of supramolecular nanostructured electrodes of porphyrin-modified TiO_2 nanoparticles with fullerene [OTE/SnO_2/(**Ar-H_2P-COO-TiO_2**+C_{60})$_n$, OTE/SnO_2/(**H-H_2P-COO-TiO_2**+C_{60})$_n$ and OTE/SnO_2/(**H_2P-4COO-TiO_2**+C_{60})$_n$] are much larger than those of the reference systems of porphyrin-modified TiO_2 nanoparticles without C_{60} [OTE/SnO_2/(**Ar-H_2P-COO-TiO_2**)$_n$, OTE/SnO_2/(**H-H_2P-COO-TiO_2**)$_n$ and OTE/SnO_2/(**H_2P-4COO-TiO_2**)$_n$]. In particular, the maximum IPCE value (41%) is obtained for OTE/SnO_2/(**H-H_2P-COO-TiO_2**+C_{60})$_n$ under the bias potential of 0.2 V *vs*. SCE. This indicates that the formation of supramolecular complexes between porphyrins and fullerene on TiO_2 nanoparticles plays an important role in improvement of the light energy conversion properties.

Introduction

Increasing attention has been attracted toward the solar energy to current conversion to develop inexpensive and efficient solar cells.[1-6] The construction of such efficient photovoltaic devices requires an enhanced light-harvesting efficiency of chromophore molecules throughout the solar spectrum together with a highly efficient conversion of the harvested light into electrical energy.[1-6]

Porphyrinoid chromophores have been involved in a number of important biological electron-transfer systems including the primary photochemical reactions of chlorophylls in the photosynthetic reaction centers.[7] Rich and extensive absorption features of porphyrinoid systems result in increased absorption cross-sections and an efficient use of the solar spectrum.[8-10] In purple photosynthetic bacteria, visible light is thereby harvested efficiently by the antenna complexes composed of a wheel-like array of chlorophylls.[11] Since porphyrins contain an extensively conjugated two-dimensional π-system, they are suitable not only for synthetic light-harvesting systems, but also for efficient electron transfer, because the uptake or release of electrons results in minimal structural and solvation change upon electron transfer.[12] In contrast with the two-dimensional porphyrin π-system, fullerenes contain an extensively conjugated three-dimensional π system.[13-15] Buckminsterfullerene (C_{60}), for example, is described as having a closed-shell configuration consisting of 30 bonding molecular orbitals with 60 π-electrons,[13-15] which is also suitable for the efficient electron-transfer reduction because of the minimal changes of structure and solvation associated with the electron transfer.[16] Judging from the excellent light harvesting properties of porphyrins and the efficient electron-transfer properties of both porphyrins and fullerenes, combination of porphyrins and fullerenes seems to be ideal for fulfilling an enhanced light-harvesting efficiency of chromophores throughout the solar spectrum and a highly efficient conversion of the harvested light into the photocurrent generation. In

addition, porphyrins are known to form supramolecular complexes with C_{60}, which contain closest contacts between one of the electron-rich 6:6 bonds of the guest fullerene and the geometric center of the host porphyrins.[17-20] The strong interaction between porphyrins and fullerenes is likely to be a good driving force for the formation of supramolecular complexes between porphyrins and C_{60}.[21] Self-assembled monolayers (SAMs) of fullerenes and porphyrins have thereby merited special attention as artificial photosynthetic materials and photonic molecular devices.[22-24] However, such monolayer assemblies possess poor light-harvesting capability, affording only low values of the incident photon-to-photocurrent efficiency (IPCE). In addition, the synthetic difficulty has precluded practical application of such artificial photosynthetic model compounds to develop low-cost photovoltaic devices.

In order to overcome these problems, we have previously reported a simple and new approach to prepare composite clusters of porphyrins and fullerene in a mixture of polar and nonpolar solvents, which are assembled as multilayers on a nanostructured SnO_2 electrode using an electrophoretic deposition technique.[25] The photoelectrochemical properties of the composite systems of porphyrins and fullerene are superior to those of the single component system.[25a] In particular, multi-porphyrin arrays such as porphyrin dendrimers and porphyrin-modified gold nanoclusters with fullerenes exhibit much improved photoelectrochemical properties as compared with the composite clusters of monomeric porphyrin and fullerene.[26]

On the other hand, assembly of dye-modified TiO_2 nanoparticles on electrodes using the electrophoretic deposition technique has also been reported to be useful for preparation of organic thin films to obtain good electron acceptor materials.[3c,d,27,28] The electrophoretic deposition of dye-modified TiO_2 nanoparticles on electrodes is an attractive method for preparation of organic multilayer films. However, assembly of porphyrin-modified TiO_2

nanoparticles on electrodes using the electrophoretic deposition technique has yet to be applied to construct the supramolecular electrodes with C_{60}.

We report herein a new type of organic solar cells based on composite nanoclusters of porphyrin-modified TiO_2 nanoparticles and fullerene and the photoelectrochemical properties, which are different depending on the type of porphyrins shown in Figure 1: 5-[4-benzoic acid]-10,15,20-tris[3,5-di-*tert*-butylphenyl]-21*H*,23*H*-porphyrin (**Ar-H_2P-COOH**), 5-[4-benzoic acid]-10,20-di[3,5-di-*tert*-butylphenyl]-21*H*,23*H*-porphyrin (**H-H_2P-COOH**), 5,10,15,20-tetra[4-benzoic acid]-21*H*,23*H*-porphyrin (**H_2P-4COOH**). The porphyrin (**H_2P)** moieties are modified with carboxylic acid group (**Ar-H_2P-COOH, H-H_2P-COOH** and **H_2P-4COOH** in Figure 1) in order to be assembled on TiO_2 nanoparticles [denoted as **Ar-H_2P-COO-TiO_2**, **H-H_2P-COO-TiO_2** and **H_2P-4COO-TiO_2** in Figure 1, respectively].

Figure 1

The porphyrin-modified TiO_2 nanoparticles and fullerene nanoclusters are deposited as thin films on optically transparent electrode (OTE) of nanostructured SnO_2 (OTE/SnO_2) using an electrophoretic method as shown in Scheme 1. We examined the photoelectrochemical properties of composite cluster system using porphyrin-modified TiO_2 nanoparticles (**Ar-H_2P-COO-TiO_2, H-H_2P-COO-TiO_2** and **H_2P-4COO-TiO_2**) and fullerene (C_{60}) on OTE/SnO_2 electrode [denoted as OTE/SnO_2/(**Ar-H_2P-COO-TiO_2**+C_{60})$_n$, OTE/SnO_2/(**H-H_2P-COO-TiO_2**+C_{60})$_n$ and OTE/SnO_2/(**H_2P-4COO-TiO_2**+C_{60})$_n$, respectively] relative to the reference systems containing porphyrin-modified TiO_2 nanoparticles without C_{60} [OTE/SnO_2/(**Ar-H_2P-COO-TiO_2**)$_n$, OTE/SnO_2/(**H-H_2P-COO-TiO_2**)$_n$ and OTE/SnO_2/(**H_2P-4COO-TiO_2**)$_n$]. The morphology and light energy conversion

properties including the mechanism of these composite cluster systems are described in full detail in this paper.

Scheme 1

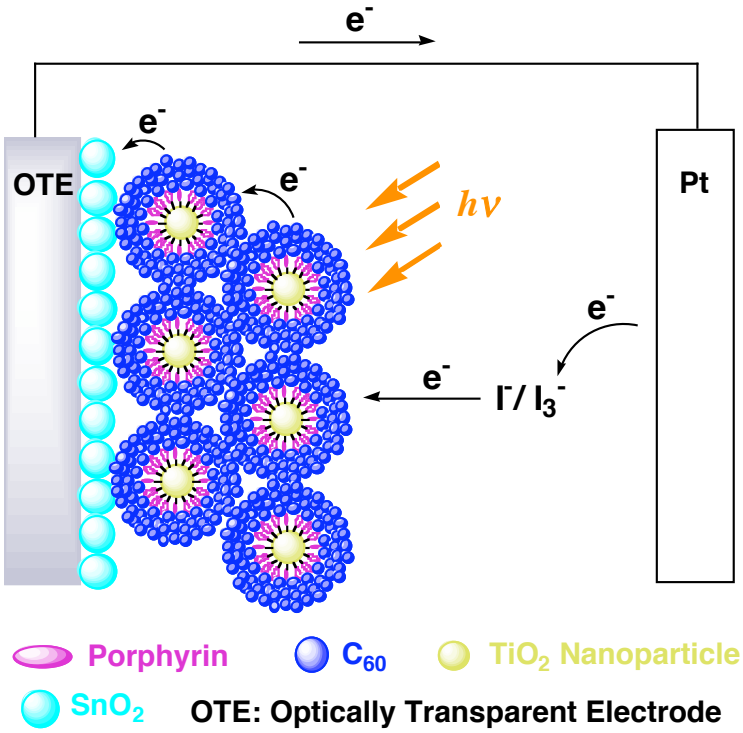

Experimental Section

General. Chemicals used in this study are of the best grade available, supplied by Tokyo Chemical Industries, Wako Pure Chemical, or Sigma Aldrich Co. ^{1}H NMR spectra were recorded on a JNM-AL300 (JEOL) instrument at 300 MHz. Matrix-assisted laser desorption/ionization (MALDI) time-of-flight (TOF) mass spectra were measured on a Kratos Compact MALDI I (Shimadzu). TiO_2 nanoparticles (P25, d = 21 nm) were purchased from Nippon Aerogel Co. **H_2P-4COOH** was purchased from Sigma Aldrich Co. Preparation of **Ar-H_2P-COOH** and **H-H_2P-COOH** have been described elsewhere.[29,30]

Preparation of TiO_2 nanoparticles modified with porphyrin moieties. TiO_2 nanoparticles modified with porphyrin moieties (**Ar-H_2P-COO-TiO_2**, **H-H_2P-COO-TiO_2** and **H_2P-4COO-TiO_2**) were prepared by immersing warmed TiO_2 nanoparticles (80 ~ 100 °C) in acetonitrile (10 mL) containing 3.0×10^{-4} mol dm^{-3} of **Ar-H_2P-COOH**, **H-H_2P-COOH** and **H_2P-4COOH** for 12 h, respectively. After adsorbing **Ar-H_2P-COOH**, **H-H_2P-COOH** and **H_2P-4COOH**, TiO_2 nanoparticles were filtered, and the subsequent washing with acetonitrile and drying afforded **Ar-H_2P-COO-TiO_2**, **H-H_2P-COO-TiO_2** and **H_2P-4COO-TiO_2**, respectively. The dye molecules were completely desorbed from TiO_2 nanoparticles into solution by immersing the dye-modified TiO_2 nanoparticles in methanol overnight. The amounts of **Ar-H_2P-COOH**, **H-H_2P-COOH** and **H_2P-4COOH** adsorbed on TiO_2 nanoparticles relative to the total weight were determined as 2.98×10^{-5}, 2.98×10^{-5}, and 2.97×10^{-5} mol/g, respectively.[28] The molecular packing densities of porphyrins on TiO_2 nanoparticles are approximately the same.

Electrophoretic deposition of composite clusters on electrode. C_{60} is soluble in nonpolar solvents such as toluene. In mixed solvents (acetonitrile/toluene), however, they aggregate to form large size clusters with diameter of 100 nm - 300 nm.[31] The C_{60} cluster and TiO_2 nanoparticles were electrophoretically deposited onto SnO_2 films under an applied potential as reported previously.[28,31]

Nanostructured SnO_2 films were cast on an optically transparent electrode (OTE) by using a dilute (1-2%) colloidal solution (Alfa Chemicals), followed by annealing of the dried film at 673 K. Details about the electrode preparation and its properties have been described elsewhere.[32] These films are highly porous and electrochemically active to conduct charges across the film. The SnO_2 film electrode (OTE/SnO_2) and an OTE plate were introduced in a 1 cm path length cuvette and were connected to positive and negative terminals of the power supply, respectively. A known amount (~2 mL) of C_{60}, porphyrin-

modified TiO_2 nanoparticles (**Ar-H_2P-COO-TiO_2**, **H-H_2P-COO-TiO_2** and **H_2P-4COO-TiO_2**), or the mixed cluster suspension in acetonitrile/toluene (3/1, v/v) immediately after the ultrasonication was transferred to a 1 cm cuvette in which two electrodes (viz., OTE/SnO_2 and OTE) were kept at a distance of ~6 mm using a Teflon spacer. A dc voltage (500 V) was applied between the two electrodes for 2 min using a Fluke 415 power supply. The deposition of the film can be visibly seen as the solution becomes colorless with simultaneous brown coloration of the SnO_2/OTE electrode. The SnO_2/OTE electrodes coated with porphyrin-modified TiO_2 nanoparticles (**Ar-H_2P-COO-TiO_2**, **H-H_2P-COO-TiO_2** and **H_2P-4COO-TiO_2**) and C_{60} clusters are referred to OTE/SnO_2/(**Ar-H_2P-COO-TiO_2**+C_{60})$_n$, OTE/SnO_2/(**H-H_2P-COO-TiO_2**+C_{60})$_n$, and OTE/SnO_2/(**H_2P-4COO-TiO_2**+C_{60})$_n$, respectively.

The UV-visible spectra were recorded on a Shimadzu 3101 spectrophotometer. Images were recorded using a Hitachi H600 transmission electron microscope. The morphology of the mesoporous electrodes was characterized by a scanning electron micrograph (SEM; JEOL, JSM-6700F).

Photoelectrochemical measurements. Photoelectrochemical measurements were performed using a standard three-compartment cell consisting of a working electrode and Pt wire gauze counter electrode and saturated calomel reference electrode (SCE). All photoelectrochemical measurements were performed in acetonitrile containing 0.5 mol dm^{-3} NaI and 0.01 mol dm^{-3} I_2 with a Keithley model 617 programmable electrometer. A collimated light beam from a 150 W Xenon lamp with a 400 nm cut-off filter was used for excitation of the composite cluster films cast on SnO_2 electrodes. A Bausch and Lomb high intensity grating monochromator was introduced into the path of the excitation beam for selecting wavelength. A Princeton Applied Research (PAR) model 173 potentiostat and Model 175 universal programmer were used for recording I-V characteristics. The IPCE

values were calculated by normalizing the photocurrent values for incident light energy and intensity using eqn. (1),[25]

$$\text{IPCE}\ (\%) = 100 \times 1240 \times I_{sc}/(W_{in} \times \lambda) \qquad (1)$$

where I_{sc} is the short circuit photocurrent (A/cm^2), W_{in} is the incident light intensity (W/cm^2), and λ is the wavelength (nm).

Results and discussion

Preparation of the composite cluster films of porphyrin-modified TiO_2 nanoparticles and C_{60}. Porphyrins and C_{60} are soluble in nonpolar solvents such as toluene, but much less soluble in polar solvents such as acetonitrile.[25,26] By the proper choice of polar to nonpolar solvent, we can achieve a controlled aggregation in the form of the composite nanoclusters. Detailed information of composite nanoclusters of porphyrins and C_{60} has been described elsewhere.[25,31] TiO_2 nanoparticles were electrophoretically deposited onto the electrode in suspended solution.[28] Upon subjecting the resultant cluster suspension to a high electric dc field (500 V for 2 min), mixed porphyrin-modified TiO_2 nanoparticles (**Ar-H_2P-COO-TiO_2**, **H-H_2P-COO-TiO_2** and **H_2P-4COO-TiO_2**) and fullerene clusters [(**H_2P-COO-TiO_2+C_{60})$_n$**] were deposited onto an optically transparent electrode (OTE) of a nanostructured SnO_2 electrode (OTE/SnO_2), to afford the modified electrode. As the deposition continues we can visually observe decoloration of the solution, accompanied by coloration of the electrode that is connected to positive terminal of the dc power supply. A mixed cluster suspension of porphyrin-modified TiO_2 nanoparticles (**Ar-H_2P-COO-TiO_2**, **H-H_2P-COO-TiO_2** and **H_2P-4COO-TiO_2**) and C_{60} were prepared in the

total concentration range from 0.025 to 0.13 mmol dm^{-3} (molecular ratio of **H_2P**:C_{60} = 1:5) in acetonitrile/toluene (3/1, v/v). In this case, the mixed clusters were first prepared using different amounts of **H_2P** on TiO_2 nanoparticle and C_{60} to maintain their molar ratio as 1:5. The absorption spectrum of OTE/SnO_2/(**H_2P-4COO-TiO_2**+C_{60})$_n$ shows that incident light is absorbed strongly in the visible and near-infrared regions (spectrum a in Figure 2). A broad absorption is observed in OTE/SnO_2/(**H_2P-4COO-TiO_2**+C_{60})$_n$ in the visible region as compared with the reference system without C_{60} [OTE/SnO_2/(**H_2P-4COO-TiO_2**)$_n$]. Such a broad absorption property of OTE/SnO_2/(**H_2P-COO-TiO_2**+C_{60})$_n$ may be ascribed to charge-transfer (CT) absorption between porphyrins and C_{60}.[25,26,33] Absorption properties of OTE/SnO_2/(**Ar-H_2P-COO-TiO_2**+C_{60})$_n$ and OTE/SnO_2/(**H-H_2P-COO-TiO_2**+C_{60})$_n$ are similar to that of OTE/SnO_2/(**H_2P-4COO-TiO_2**+C_{60})$_n$.

Figure 2

Morphology of OTE/SnO_2/(H-H_2P-COO-TiO_2+C_{60})$_n$. Scanning electron micrograph (SEM) was used to examine the morphology of the OTE/SnO_2/(**H-H_2P-COO-TiO_2**+C_{60})$_n$ film as shown in Figure 3. The OTE/SnO_2/(**H-H_2P-COO-TiO_2**+C_{60})$_n$ film is composed of closely packed clusters of about 20-200 nm size with a networked structure, which may result from a supramolecular CT interaction between **H_2P** and C_{60} on TiO_2 nanoparticles. In contrast with the OTE/SnO_2/(**H-H_2P-COO-TiO_2**+C_{60})$_n$ film, the OTE/SnO_2/(C_{60})$_n$ film without porphyrin-modified TiO_2 nanoparticles contain a large size (100 – 300 nm) of nanoclusters as reported previously.[28,31b] Based on these SEM images we can conclude that TiO_2 nanoparticles play an important role in the cluster formation on the films.

Figure 3

Photoelectrochemical properties of the composite cluster films of porphyrin-modified TiO_2 nanoparticles and C_{60} on OTE/SnO_2 electrodes. The photoelectrochemical performance was examined using the composite cluster films of porphyrin-modified TiO_2 nanoparticles (**Ar-H_2P-COO-TiO_2**, **H-H_2P-COO-TiO_2**, and **H_2P-4COO-TiO_2**) and C_{60} as a photoanode in a photoelectrochemical cell. Photocurrent measurements were performed in acetonitrile containing NaI (0.5 mol dm^{-3}) and I_2 (0.01 mol dm^{-3}) as redox electrolyte and Pt gauge counter electrode. The photovoltage and photocurrent responses recorded following the excitation of OTE/SnO_2/(**H-H_2P-COO-TiO_2**+C_{60})$_n$ electrode the visible light region ($\lambda > 400$ nm) are shown in Figure 4A and B, respectively. The photocurrent response is prompt, steady and reproducible during repeated on/off cycles of the visible light illumination. The short circuit photocurrent density (I_{sc}) is 0.095 mA/cm^2, and open circuit voltage (V_{oc}) is 240 mV were reproducibly obtained during these measurements. Blank experiments conducted with OTE/SnO_2 (i.e., by excluding composite clusters (**H-H_2P-COO-TiO_2**+C_{60})$_n$) produced no detectable photocurrent under the similar experimental conditions. These experiments confirmed the important role of (**H-H_2P-COO-TiO_2**+C_{60})$_n$ assembly towards harvesting light energy and generating photocurrent during the operation of a photoelectrochemical cell.

Figure 4

The charge separation in the OTE/SnO_2/(**H-H_2P-COO-TiO_2**+C_{60})$_n$ electrode can be further modulated by the application of an electrochemical bias potential. Figure 5 shows *I-V* characteristics of the OTE/SnO_2/(**H-H_2P-COO-TiO_2**+C_{60})$_n$ and OTE/SnO_2/(**H-H_2P-COO-TiO_2**)$_n$ electrodes under the visible light illumination. The photocurrent increases as

the applied potential is scanned towards more positive potentials. Increased charge separation and the facile transport of charge carriers under a positive bias potential are responsible for enhanced photocurrent generation. The ratio of net photocurrent generation of OTE/SnO_2/(**H-H_2P-COO-TiO_2**+C_{60})$_n$ at +0.2 V *vs*. SCE to that of OTE/SnO_2/(**H-H_2P-COO-TiO_2**+C_{60})$_n$ at 0 V *vs*. SCE (Figure 5A) is much larger than the case of OTE/SnO_2/(**H-H_2P-COO-TiO_2**)$_n$ (Figure 5B). This demonstrates that C_{60} works as an electron acceptor in the supramolecular complex to enhance the photocurrent generation. At potentials greater than +0.4 V *vs*. SCE, the direct electrochemical oxidation of iodide interferes with the photocurrent measurement.

Figure 5

A series of photocurrent action spectra were recorded in order to evaluate the photoresponse of the composite clusters towards the photocurrent generation. First, we measured the photocurrent action spectra of OTE/SnO_2/(**Ar-H_2P-COO-TiO_2**)$_n$, OTE/SnO_2/(**H-H_2P-COO-TiO_2**)$_n$ and OTE/SnO_2/(**H_2P-4COO-TiO_2**)$_n$ as shown in Figure 6. Photocurrent generation is observed under no applied bias potential using a standard two-compartment cell consisting of a working electrode and Pt wire gauze counter electrode to attain 2~6% of maximum IPCE values (spectra a in Figure 6A, 6B and 6C, respectively). We also measured the photocurrent action spectra of OTE/SnO_2/(**Ar-H_2P-COO-TiO_2**)$_n$, OTE/SnO_2/(**H-H_2P-COO-TiO_2**)$_n$ and OTE/SnO_2/(**H_2P-4COO-TiO_2**)$_n$ under an applied bias potential of 0.2 V *vs*. SCE using a standard three-compartment cell as a working electrode along with Pt wire gauze counter electrode and saturated calomel reference electrode (SCE) (spectra b in Figure 6A, 6B and 6C, respectively). The maximum IPCE value (~20%) is obtained for OTE/SnO_2/(**H_2P-4COO-TiO_2**)$_n$, which is much larger than those of

OTE/SnO_2/(**Ar-H_2P-COO-TiO_2**)$_n$ (~3.5%) and OTE/SnO_2/(**H-H_2P-COO-TiO_2**)$_n$ (~6%). This demonstrates that the difference in the IPCE values results from different electron injection properties from the excited state of porphyrins to the conduction band of TiO_2 semiconductor nanocrystallites. From the structural point of view between porphyrin moieties and TiO_2 nanoparticles, porphyrin moieties definitely lie on the TiO_2 surface because of four-point connection in the case of **H_2P-4COO-TiO_2**, whereas porphyrin moieties may stand on the TiO_2 surface in the cases of OTE/SnO_2/(**Ar-H_2P-COO-TiO_2**)$_n$ and OTE/SnO_2/(**H-H_2P-COO-TiO_2**)$_n$ as shown in Figure 1. The close distance between porphyrins and TiO_2 surface in **H_2P-4COO-TiO_2** relative to that of **Ar-H_2P-COO-TiO_2** or **H-H_2P-COO-TiO_2** may result in an efficient electron transfer from the excited state of the porphyrin moiety of **H_2P-4COO-TiO_2** to the conduction band of TiO_2 semiconductor nanocrystallites.

Figure 6

We have also measured the photocurrent action spectra of OTE/SnO_2/(**Ar-H_2P-COO-TiO_2**+C_{60})$_n$, OTE/SnO_2/(**H-H_2P-COO-TiO_2**+C_{60})$_n$ and OTE/SnO_2/(**H_2P-4COO-TiO_2**+C_{60})$_n$ in order to evaluate the effect of C_{60} on the IPCE values as shown in Figure 7. IPCE values of these composite cluster systems under an applied bias potential of 0.2 V *vs*. SCE become larger than those under no applied potential, as observed for porphyrin-modified TiO_2 nanoparticle films without C_{60} (Figure 6). The IPCE values of composite cluster electrodes (Figure 7A, B and C) also become larger than those of the individual systems [OTE/SnO_2/(C_{60})$_n$ (Figure 7D) or OTE/SnO_2/(porphyrin-modified TiO_2 nanoparticle)$_n$ (Figure 6)]. In particular, the maximum IPCE value of OTE/SnO_2/(**H-H_2P-COO-TiO_2**+C_{60})$_n$ under the bias of 0.2 V *vs*. SCE (~42%) is much larger than the sum of two

individual IPCE values (spectrum c in Figure 7B: ~12%) of OTE/SnO_2/(**H-H_2P-COO-TiO_2**)$_n$ (spectrum b in figure 6B) and OTE/SnO_2/(C_{60})$_n$ (spectrum b in Figure 7D) with the same concentrations of **H_2P** and C_{60}. This indicates that the interaction between **H_2P** and C_{60} contributes significantly to an increase in the IPCE value.

Figure 7

We have further compared the action spectrum of OTE/SnO_2/(**H-H_2P-COO-TiO_2**+C_{60})$_n$ with those of OTE/SnO_2/(**Ar-H_2P-COO-TiO_2**+C_{60})$_n$ and OTE/SnO_2/(**H_2P-4COO-TiO_2**+C_{60})$_n$. It should be noted that the molecular packing densities of porphyrins on TiO_2 nanoparticles are approximately the same in OTE/SnO_2/(**H-H_2P-COO-TiO_2**+C_{60})$_n$, OTE/SnO_2/(**Ar-H_2P-COO-TiO_2**+C_{60})$_n$ and OTE/SnO_2/(**H_2P-4COO-TiO_2**+C_{60})$_n$ (vide supra). In the case of comparison between OTE/SnO_2/(**H-H_2P-COO-TiO_2**+C_{60})$_n$ and OTE/SnO_2/(**Ar-H_2P-COO-TiO_2**+C_{60})$_n$ under the bias of 0.2 V *vs*. SCE, the IPCE value of OTE/SnO_2/(**H-H_2P-COO-TiO_2**+C_{60})$_n$ (spectrum b in Figure 7B) is much larger than that of OTE/SnO_2/(**Ar-H_2P-COO-TiO_2**+C_{60})$_n$ (spectrum b in Figure 7A). The absence of 3,5-di-*tert*-butylphenyl substituent at the 15-*meso* position of porphyrin ring in **H-H_2P-COO-TiO_2** may enhance the interaction with C_{60}, which can be inserted between two porphyrin rings of the porphyrin assembly on TiO_2 nanoparticles (Scheme 2), as compared with **Ar-H_2P-COO-TiO_2** in which the *meso* positions are fully substituted. The stronger interaction between the less bulky porphyrins and C_{60} leads to an increase in the IPCE value. Such a sandwiched structure of C_{60} inserted between two porphyrin rings in Scheme 2 may be impossible in the case of OTE/SnO_2/(**H_2P-4COO-TiO_2**+C_{60})$_n$ because of the four-point connection of the porphyrin ring onto the TiO_2 surface. This may be the reason why the IPCE values of OTE/SnO_2/(**H_2P-4COO-TiO_2**)$_n$ under an applied bias potential of 0.2 V *vs*.

SCE (spectrum b in Figure 7C) are smaller than those of OTE/SnO_2/(**H-H_2P-COO-TiO_2**)$_n$ (spectrum b in Figure 7B).[34] Based on these results, we can conclude that three dimensional steric control between donor and acceptor moieties is a key factor for construction of efficient organic solar devices.

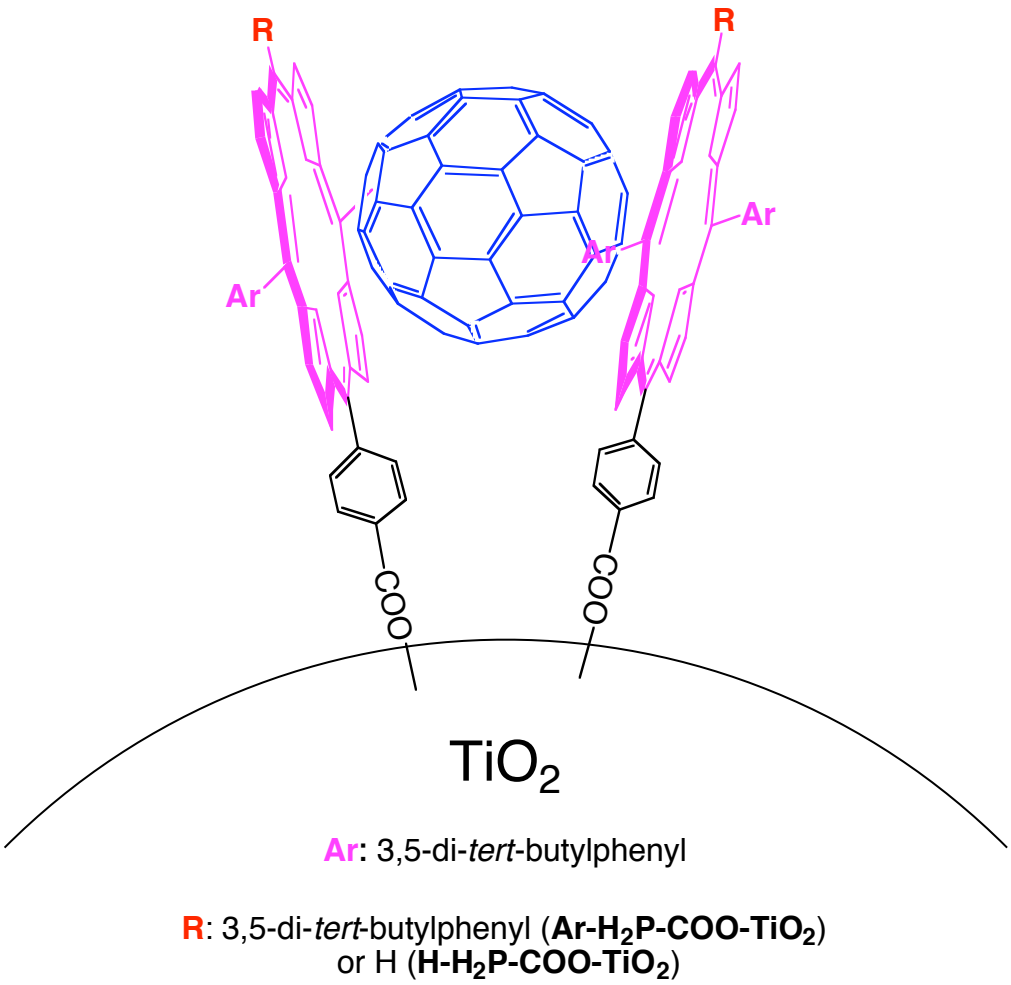

Scheme 2. Illustration of supramolecular assembly between porphyrins and C_{60} in (**Ar-H_2P-COO-TiO_2**+C_{60})$_n$ and (**H-H_2P-COO-TiO_2**+C_{60})$_n$.

Power conversion efficiency. The power conversion efficiency (η) of the photoelectrochemical cell was determined by varying the load resistance with use of eqn. (2),[25a]

$$\eta = ff \text{ x } I_{sc} \text{ x } V_{oc}/W_{in} \quad (2)$$

where the fill factor (*ff*) is defined as $ff = P_{max}/(V_{oc} \times I_{sc})$; P_{max} is the maximum power output of the cell, V_{oc} is the open circuit photovoltage, I_{sc} is the short circuit photocurrent. A decrease in the photovoltage accompanied by an increase in the photocurrent is observed with decreasing the load resistance as shown in Figure 8. The detailed characteristics of the

Figure 8

OTE/SnO_2/(**H-H_2P-COO-TiO_2**)$_n$, OTE/SnO_2/(**H-H_2P-COO-TiO_2**+C_{60})$_n$ and OTE/-SnO_2/(**H_2P-4COO-TiO_2**+C_{60})$_n$ electrodes are summarized in Table 1. The I_{sc} and V_{oc} values of OTE/SnO_2/(**H-H_2P-COO-TiO_2**+C_{60})$_n$ are much larger than those of OTE/SnO_2/(**H-H_2P-COO-TiO_2**)$_n$, leading to more than 4 times improvement of the η value (0.11%) as compared with that of OTE/SnO_2/(**H-H_2P-COO-TiO_2**)$_n$ (0.025%). Furthermore, the η value of highly organized OTE/SnO_2/(**H-H_2P-COO-TiO_2**+C_{60})$_n$ using TiO_2 nanoparticles is about 3 times larger than that of non-organized composite cluster system of porphyrin and fullerene without TiO_2 nanoparticles, which was reported previously (~0.03%).[25a,26a,b] The η value of OTE/SnO_2/(**H_2P-4COO-TiO_2**+C_{60})$_n$ (0.10%) is about the same as that of OTE/SnO_2/(**H-H_2P-COO-TiO_2**+C_{60})$_n$ (0.11%).

Table 1

Photocurrent generation mechanism. The photocurrent generation mechanism in composite cluster systems of porphyrin and fullerene has previously been reported to be initiated by ultrafast electron transfer from the singlet excited state of porphyrin to C_{60} in the femtosecond time domain.[25,26] In the case of the reference systems without C_{60} [OTE/SnO_2/(**Ar-H_2P-COO-TiO_2**)$_n$, OTE/SnO_2/(**H-H_2P-COO-TiO_2**)$_n$, and OTE/SnO_2/-(**H_2P-4COO-TiO_2**)$_n$], the photoexcitation of **H_2P** moiety results in electron injection from the singlet excited state of the dye into the conduction band and/or trap states of TiO_2 nanoparticles to produce the porphyrin radical cation (**$H_2P^{\bullet+}$**). The electrons collected on TiO_2 nanoparticles are furthermore injected into SnO_2 nanocrystallites (E_{CB} = 0 V *vs.* NHE)[25a] to produce the photocurrent in the circuit. The resulting porphyrin radical cation (**$H_2P^{\bullet+}$**) produced in the photoinduced electron injection to the conduction band of TiO_2 is reduced by electrolyte (I_3^-/I^- = 0.5 V *vs.* NHE) in the multilayer film.[25] At the counter electrode, the electron reduces the oxidized electrolyte (I_3^-), leading to the photocurrent generation.

In the cases of OTE/SnO_2/(**H-H_2P-COO-TiO_2**+C_{60})$_n$, OTE/SnO_2/(**H-H_2P-COO-TiO_2**+C_{60})$_n$ and OTE/-SnO_2/(**H_2P-4COO-TiO_2**+C_{60})$_n$, not only TiO_2 nanoparticles, but also C_{60} molecules ($C_{60}/C_{60}^{\bullet-}$ = -0.2 V *vs.* NHE)[25a] act as an electron acceptor, leading to the enhancement of the photocurrent generation efficiency in composite cluster systems (porphyrin-modified TiO_2 nanoparticle and C_{60}) as compared with the systems without C_{60}. The major pathway contributing to the enhanced photocurrent generation is the intermolecular charge transfer between excited **H_2P** and C_{60} within the supramolecular complex to produce **$H_2P^{\bullet+}$** and $C_{60}^{\bullet-}$. Photoinduced electron transfer from the porphyrin singlet excited state ($^1H_2P^*$) to C_{60} is thermodynamically feasible as evident from the oxidation potential of $^1H_2P^*$ ($^1H_2P^*/H_2P^{\bullet+}$ = -0.7 V *vs.* NHE),[25] which is more negative than the reduction potential of C_{60} ($C_{60}/ C_{60}^{\bullet-}$ = -0.2 V *vs.* NHE).[25a] Such photoinduced electron

transfer from the excited porphyrins to C_{60} has been well established by earlier studies.[16,26] $C_{60}^{\bullet-}$ is also generated from the interaction between excited C_{60} (C_{60}^{*}) and iodide ions present in the electrolyte. Collectively, these $C_{60}^{\bullet-}$ species accumulated in clusters transfer electrons to SnO_2 nanocrystallites (E_{CB} = 0 V *vs*. NHE),[25,31] to produce the current in the circuit. The regeneration of **H_2P** ($H_2P/H_2P^{\bullet+}$ = 1.2 V *vs*. NHE)[25] is achieved by the triiodide/iodide couple (I_3^-/I^- = 0.5 V *vs*. NHE)[25] present in the electrolyte system. The improvement of IPCE values under an applied bias potential of 0.2 V *vs*. SCE relative to the corresponding systems under no applied potential results from an increase of driving force of electron transfer from $C_{60}^{\bullet-}$ to SnO_2 nanocrystallites using a standard three-compartment cell.

Conclusion

We have successfully constructed supramolecular photovoltaic cells composed of molecular nanocluster assemblies of porphyrin and fullerene, which are well organized with TiO_2 nanoparticles. The IPCE values of the composite cluster systems of porphyrins and C_{60} with TiO_2 nanoparticles [OTE/SnO_2/(**H-H_2P-COO-TiO_2**+C_{60})$_n$, OTE/SnO_2/(**H-H_2P-COO-TiO_2**+C_{60})$_n$ and OTE/-SnO_2/(**H_2P-4COO-TiO_2**+C_{60})$_n$] are improved as compared with the reference systems [OTE/SnO_2/(**H-H_2P-COO-TiO_2**)$_n$, OTE/SnO_2/(**H-H_2P-COO-TiO_2**)$_n$ and OTE/-SnO_2/(**H_2P-4COO-TiO_2**)$_n$]. The largest η value is achieved in OTE/SnO_2/(**H-H_2P-COO-TiO_2**)$_n$ (0.11%) composed of the porphyrin-modified TiO_2 nanoparticles and C_{60} clusters.

Acknowledgment

This work was partially supported by a Grant–in–Aid (No. 16205020) and by a COE program of Osaka University (Integrated Ecochemistry) from the Ministry of Education,

Culture, Sports, Science, and Technology, Japan. PVK acknowledges the support from the Office of Basic Energy Science of the U. S. Department of the Energy. TH acknowledges the support of Japan Society for the Promotion of Science Research Fellowship for Young Scientist. This is contribution No. NDRL 4605 from the Notre Dame Radiation Laboratory and from Osaka University. We are grateful to Dr. Yuji Wada, Osaka University, for helping preparation of TiO_2 nanoparticles modified with dyes.

References and Notes

1. (a) O'Regan, B.; Grätzel, M. *Nature* **1991**, *353*, 737. (b) Bach, U.; Lupo, D.; Comte, P.; Moser, J. E.; Weissörtel, F.; Salbeck, J.; Spreitzer, H.; Grätzel, M. *Nature* **1998**, *395*, 583. (c) Hagfeldt, A.; Grätzel, M. *Chem. Rev.* **1995**, *95*, 49. (d) Hagfeldt, A.; Grätzel, M. *Acc. Chem. Res.* **2000**, *33*, 269.
2. (a) Velusamy, M.; Justin Thomas, K. R.; Lin, J. T.; Hsu, Y.-C.; Ho, K.-C. *Org. Lett.* **2005**, *7*, 1899. (b) Padinger, F.; Rittberger, R. S.; Sariciftci, N. S. *Adv. Funct. Mater.* **2003**, *13*, 85. (c) Schmidt-Mende, L.; Fechtenkötter, A.; Müllen, K.; Moons, E.; Friend, R. H.; MacKenzie, J. D. *Science* **2001**, *293*, 1119.
3. (a) Huynh, W. U.; Dittmer, J. J.; Alivisatos, A. P. *Science* **2002**, *295*, 2425. (b) Liu, J.; Tanaka, T.; Sivula, K.; Alivisatos, A. P.; Frechet, J. M. J. *J. Am. Chem. Soc.* **2004**, *126*, 6550. (c) Zhang, D.; Yoshida, T.; Minoura, H. *Chem. Lett.* **2002**, *31*, 874. (d) Zhang, D.; Yoshida, T.; Minoura, H. *Adv. Mater.* **2003**, *15*, 814.
4. (a) Bignozzi, C. A.; Argazzi, R.; Kleverlaan, C. J. *Chem. Soc. Rev.* **2000**, *29*, 87. (b) Liu, J.; Kadnikova, E. N.; Liu, Y.; McGehee, M. D.; Frechet, J. M. J. *J. Am. Chem. Soc.* **2004**, *126*, 9486. (c) Smith, Adam P.; Smith, Rachel R.; Taylor, Barney E.; Durstock, Michael F. *Chem. Mater.* **2004**, *16*, 4687.

5. (a) Yang, Fan; Shtein, Max; Forrest, Stephen R. *Nature Mater.* **4**, 37. (b) Halls, J. J. M.; Walsh, C. A.; Greenham, N. C.; Marseglia, E. A.; Friend, R. H.; Moratti, S. C.; Holmes, A. B. *Nature* **1995**, *376*, 498.
6. (a) Wienk, M. M.; Kroon, J. M.; Verhees, W. J. H.; Knol, J.; Hummelen, J. C.; van Hal, P. A.; Janssen, R. A. J. *Angew. Chem., Ind. Ed.* **2003**, *42*, 3371. (b) Peumans, P.; Uchida, S.; Forrest, S. R. *Nature* **2003**, *425*, 158. (c) Eckert, J.-F.; Nicoud, J.-F.; Nierengarten, J.-F.; Liu, S.-G.; Echegoyen, L.; Barigelletti, F.; Armaroli, N.; Ouali, L.; Krasnikov, V.; Hadziioannou, G. *J. Am. Chem. Soc.* **2000**, *122*, 7467.
7. (a) Barber, J. *Nature* **1988**, *333*, 114. (b) *The Photosynthetic Reaction Center*; Deisenhofer, J., Norris, J. R., Eds.; Academic Press: San Diego, 1993. (c) *Anoxygenic Photosynthetic Bacteria*; Blankenship, R. E.; Madigan, M. T.; Bauer, C. E., Eds.; Kluwer Academic Publishing: Dordrecht, 1995.
8. (a) Gust, D.; Moore, T. A.; Moore, A. L. *Acc. Chem. Res.* **1993**, *26*, 198. (b) Gust, D.; Moore, T. A.; Moore, A. L. *Acc. Chem. Res.* **2001**, *34*, 40. (c) Gust, D.; Moore, T. A. In *The Porphyrin Handbook*; Kadish, K. M., Smith, K. M., Guilard, R., Eds.; Academic Press: San Diego, CA, 2000; Vol. 8, pp 153-190.
9. (a) Wagner, R. W.; Lindsey, J. S. *Pure Appl. Chem.* **1996**, *68*, 1373. (b) Sazanovich, I. V.; Kirmaier, C.; Hindin, E.; Bocian, D. F.; Linsey, J. S.; Holten, D. *J. Am. Chem. Soc.* **2004**, *126*, 2664. (c) *Photoinduced Electron Transfer*; Fox, M. A., Channon, M., Eds.; Elsevier: Amsterdam, 1988.
10. (a) Bar-Haim, A.; Klafter, J.; Kopelman, R. *J. Am. Chem. Soc.* **1997**, *119*, 6197. (b) Sadamoto, R.; Tomioka, N.; Aida, T. *J. Am. Chem. Soc.* **1996**, *118*, 3978. (c) Jiang, D.-L.; Aida, T. *J. Am. Chem. Soc.* **1998**, *120*, 10895. (d) Choi, M.-S.; Aida, T.; Yamazaki, T.; Yamazaki, I. *Chem. Eur. J.* **2002**, *8*, 2668. (e) Capitosti, G. J.; Guerrero, C. D.; Binkley, D. E., Jr.; Rajesh, C. S.; Modarelli, D. A. *J. Org. Chem.* **2003**, *68*, 247. (f)

Harth, E. M.; Hecht, S.; Helms, B.; Malmstrom, E. E.; Frechet, J. M. J.; Hawker, C. J. *J. Am. Chem. Soc.* **2002**, *124*, 3926.

11. (a) McDermott, G.; Prince, S. M.; Freer, A. A.; Hawthornthwaite-Lawless, A. M.; Papiz, M. Z.; Cogdell, R. J.; Isaacs, N. W. *Nature* **1995**, *374*, 517. (b) Koepke, J.; Hu, X.; Muenke, C.; Schulten, K.; Michel, H. *Structure* **1996**, *4*, 581. (c) Pullerits, T.; Sundstrom, V. *Acc. Chem. Res.* **1996**, *29*, 381.
12. (a) Fukuzumi, S. In *The Porphyrin Handbook*, ed. Kadish, K. M., Smith, K. M., Guilard, R.; Academic Press: San Diego, 2000; Vol. 8, pp 115-152. (b) Fukuzumi, S.; Endo, Y.; Imahori, H. *J. Am. Chem. Soc.* **2002**, *124*, 10974.
13. Kroto, H. W.; Heath, J. R.; O'Brien, S. C.; Curl, R. F.; Smalley, R. E. *Nature* **1985**, *318*, 162.
14. (a) Haddon, R.C. *Acc. Chem. Res.* **1988**, *21*, 243. (b) Haddon, R.C. *Science* **1993**, *261*, 1545.
15. Echegoyen, L.; Echegoyen, L.E. *Acc. Chem. Res.* **1998**, *31*, 593.
16. (a) Fukuzumi, S.; Guldi, D. M. In *Electron Transfer in Chemistry*; Balzani, V. Ed.; Wiley-VCH: Weinheim, 2001; Vol. 2, pp 270-337. (b) Fukuzumi, S.; Imahori, H. In *Electron Transfer in Chemistry*; Balzani, V. Ed.; Wiley-VCH: Weinheim, 2001; Vol. 2, pp 927-975.
17. (a) Ishii, T.; Aizawa, N.; Yamashita, M.; Matsuzaka, H.; Kodama, T.; Kikuchi, K.; Ikemoto, I.; Iwasa, Y. *J. Chem. Soc., Dalton Trans.* **2000**, 4407. (b) Diederich, F.; Gömez-Löpez, M. *Chem. Soc. Rev.* **1999**, *28*, 263.
18. (a) Boyd, P. D. W.; Reed, C. A. *Acc. Chem. Res.* **2005**, *38*, 235. (b) Boyd, P. D. W.; Hodgson, M. C.; Rickard, C. E. F.; Oliver, A. G.; Chaker, L.; Brothers, P. J.; Bolskar, R. D.; Tham, F. S.; Reed, C. A. *J. Am. Chem. Soc.* **1999**, *121*, 10487. (c) Sun, D.; Tham, F. S.; Reed, C. A.; Chaker, L.; Burgess, M.; Boyd, P. D. W. *J. Am. Chem. Soc.* **2000**, *122*,

10704. (d) Sun, D.; Tham, F. S.; Reed, C. A.; Chaker, L.; Boyd, P. D. W. *J. Am. Chem. Soc*. **2002**, *124*, 6604.

19. (a) Olmstead, M. M.; Costa, D. A.; Maitra, K.; Noll, B. C.; Phillips, S. L.; Van Calcar, P. M.; Balch, A. L. *J. Am. Chem. Soc*. **1999**, *121*, 7090. (b) Olmstead, M. M.; de Bettencourt-Dias, A.; Duchamp, J. C.; Stevenson, S.; Marciu, D.; Dorn, H. C.; Balch, A. L. *Angew. Chem., Int. Ed*. **2001**, *40*, 1223.
20. (a) Zheng, J.-Y.; Tashiro, K.; Hirabayashi, Y.; Kinbara, K.; Saigo, K.; Aida, T.; Sakamoto, S.; Yamaguchi, K. *Angew. Chem., Int. Ed*. **2001**, *40*, 1857. (b) Eichhorn, D. M.; Yang, S.; Jarrell, W.; Baumann, T. F.; Beall, L. S.; White, A. J. P.; Williams, D. J.; Barrett, A. G. M.; Hoffman, B. M. *J. Chem. Soc., Chem. Commun*. **1995**, 1703.
21. Wang, Y.-B.; Lin, Z. *J. Am. Chem. Soc*. **2003**, *125*, 6072.
22. (a) Caldwell, W. B.; Chen, K.; Mirkin, C. A.; Babinec, S. J. *Langmuir* **1993**, *9*, 1945. (b) Shon, Y.-S.; Kelly, K. F.; Halas, N. J.; Lee, T. R. *Langmuir* **1999**, *15*, 5329. (c) Hirayama, D.; Takimiya, K.; Aso, Y.; Otsubo, T.; Hasobe, T.; Yamada, H.; Imahori, H.; Fukuzumi, S.; Sakata, Y. *J. Am. Chem. Soc*. **2002**, *124*, 532.
23. (a) Lahav, M.; Gabriel, T.; Shipway, A. N.; Willner, I. *J. Am. Chem. Soc*. **1999**, *121*, 258. (b) Hutchison, J. E.; Postlethwaite, T. A.; Chen, C.-h.; Hathcock, K. W.; Ingram, R. S.; Ou, W.; Linton, R. W.; Murray, R. W.; Tyvoll, T. A.; Chng, L. L.; Collman, J. P. *Langmuir* **1997**, *13*, 2143. (c) Gryko, D. T.; Zhao, F.; Yasseri, A. A.; Roth, K. M.; Bocian, D. F.; Kuhr, W. G.; Lindsey, J. S. *J. Org. Chem*. **2000**, *65*, 7356.
24. (a) Imahori, H.; Norieda, H.; Yamada, H.; Nishimura, Y.; Yamazaki, I.; Sakata, Y.; Fukuzumi, S. *J. Am. Chem. Soc*. **2001**, *123*, 100. (b) Imahori, H.; Hasobe, T.; Yamada, H.; Nishimura, Y.; Yamazaki, I.; Fukuzumi, S. *Langmuir* **2001**, *17*, 4925. (c) Hasobe, T.; Imahori, H.; Ohkubo, K.; Yamada, H.; Sato, T.; Nishimura, Y.; Yamazaki, I.; Fukuzumi, S. *J. Porphyrins Phthalocyanines* **2003**, *7*, 296.

25. (a) Hasobe, T.; Imahori, H.; Fukuzumi, S.; Kamat, P. V. *J. Phys. Chem. B* **2003**, *107*, 12105. (b) Hasobe, T.; Imahori, H.; Fukuzumi, S.; Kamat, P. V. *J. Mater. Chem.* **2003**, *13*, 2515.

26. (a) Hasobe, T.; Imahori, H.; Kamat, P. V.; Fukuzumi, S. *J. Am. Chem. Soc*. **2003**, *125*, 14962. (b) Hasobe, T.; Kashiwagi, Y.; Absalom, M. A.; Sly, J.; Hosomizu, K.; Crossley, M. J.; Imahori, H.; Kamat, P. V.; Fukuzumi, S. *Adv. Mater*. **2004**, *16*, 975. (c) Hasobe, T.; Kamat, P. V.; Troiani, V.; Solladie, N.; Ahn, T. K.; Kim, S. K.; Kim, D.; Kongkanand, A.; Kuwabata, S.; Fukuzumi, S. *J. Phys. Chem. B*. **2005**, *109*, 19. (d) Hasobe, T.; Imahori, H.; Kamat, P. V.; Ahn, T. K.; Kim, S. K.; Kim, D.; Fujimoto, A.; Hirakawa, T.; Fukuzumi, S. *J. Am. Chem. Soc*. **2005**, *127*, 1216.

27. (a) Matsumoto, Y.; Noguchi, M.; Matsunaga, T.; Kamada, K.; Koinuma, M.; Yamada, S. *Electrochemistry* **2001**, *69*, 314. (b) Miyasaka, T.; Kijitori, Y.; Murakami, T. N.; Kimura, M.; Uegusa, S. *Chem. Lett.* **2002**, *31*, 1250. (c) Xu, D.; Xu, Y.; Chen, D.; Guo, G.; Gui, L.; Tang, Y. *Adv. Mater*. **2000**, *12*, 520.

28. Hasobe, H.; Hattori, S.; Kamat, P. V.; Wada, Y.; Fukuzumi, S. *J. Mater. Chem.* **2005**, *15*, 372 .

29. Hasobe, T.; Imahori, H.; Yamada, H.; Sato, T.; Ohkubo, K.; Fukuzumi, S. *Nano Lett*. **2003**, *3*, 409.

30. Yamada, H.; Imahori, H.; Nishimura, Y.; Yamazaki, I.; Ahn, T. K.; Kim, S. K.; Kim, D.; Fukuzumi, S. *J. Am. Chem. Soc*. **2003**, *125*, 9129.

31. (a) Kamat, P. V.; Barazzouk, S.; Thomas, K. G.; Hotchandani, S. *J. Phys. Chem. B* **2000**, *104*, 4014. (b) Barazzouk, S.; Hotchandani, S.; Kamat, P. V. *Adv. Mater*. **2001**, *13*, 1614.

32. Bedja, I.; Hotchandani, S.; Kamat, P. V. *J. Phys. Chem.* **1994**, *98*, 4133.

33. Tkachenko, N. V.; Lemmetyinen, H.; Sonoda, J.; Ohkubo, K.; Sato, T.; Imahori, H.; Fukuzumi, S. *J. Phys. Chem. A*. **2003**, *107*, 8834.
34. The IPCE values in Figure 7C are particularly smaller than those in Figure 7B in the longer wavelength region because of the more unfavorable interaction between **H_2P-4COO-TiO_2** and C_{60} as compared with that between **H-H_2P-COO-TiO_2** and C_{60}.

Table 1. Performance characteristics of OTE/SnO_2/(**H-H_2P-COO-TiO_2**)$_n$, OTE/SnO_2-/(**H-H_2P-COO-TiO_2**+C_{60})$_n$, and OTE/SnO_2/(**H_2P-4COO-TiO_2**+C_{60})$_n$

System	V_{oc} (mV)	I_{sc} (mA cm^{-2})	*ff*	η (%)[a]
(H-H_2P-COO-TiO_2)$_n$	160	0.035	0.31	0.025
(H-H_2P-COO-TiO_2+C_{60})$_n$	240	0.095	0.33	0.11
(H_2P-4COO-TiO_2+C_{60})$_n$	220	0.11	0.29	0.10

[a] Electrolyte: 0.5 mol dm^{-3} NaI and 0.01 mol dm^{-3} in acetonitrile; white light illumination (λ > 400 nm); input power; 6.8 mW cm^{-2}.

Figure Captions

Figure 1. TiO_2 nanoparticles modified with porphyrin dyes and the reference compounds employed in this study.

Figure 2. (A) Absorption spectra of (a) OTE/SnO_2/(**H_2P-4COO-TiO_2**+C_{60})$_n$ ([**H_2P**] = 0.025 mmol dm^{-3}, [C_{60}] = 0.13 mmol dm^{-3}), (b) OTE/SnO_2/(**H_2P-4COO-TiO_2**)$_n$ ([**H_2P**] = 0.025 mmol dm^{-3}), (c) **H_2P-4COOH** in toluene/*tert*-butanol (v/v, 1/1) (10 μmol dm^{-3}) and (d) C_{60} in toluene (15 μmol dm^{-3}).

Figure 3. SEM (scanning electron micrograph) image of OTE/SnO_2/(**H-H_2P-COO-TiO_2**+C_{60})$_n$ ([**H_2P**] = 0.025 mmol dm^{-3}, [C_{60}] = 0.13 mmol dm^{-3}).

Figure 4. (A) Photovoltage and (B) photocurrent generation at OTE/SnO_2/(**H-H_2P-COO-TiO_2**+C_{60})$_n$ ([**H_2P**] = 0.025 mmol dm^{-3}, [C_{60}] = 0.13 mmol dm^{-3}) under illumination of white light ($\lambda > 400$ nm); electrolyte: 0.5 mol dm^{-3} NaI and 0.01 mol dm^{-3} I_2 in acetonitrile; input power: 6.8 mW cm^{-2}.

Figure 5. *I-V* characteristics of (A) OTE/SnO_2/(**H-H_2P-COO-TiO_2**+C_{60})$_n$ ([**H_2P**] = 0.025 mmol dm^{-3}, [C_{60}] = 0.13 mmol dm^{-3}) and (B) OTE/SnO_2/(**H-H_2P-COO-TiO_2**)$_n$ ([**H_2P**] = 0.025 mmol dm^{-3}) under illumination of white light ($\lambda > 400$ nm); electrolyte: 0.5 mol dm^{-3} and NaI and 0.01 mol dm^{-3} and I_2 in acetonitrile; input power: 27.8 mW cm^{-2}.

Figure 6. (A) Photocurrent action spectra of OTE/SnO_2/(**Ar-H_2P-COO-TiO_2**)$_n$ ([**H_2P**] = 0.025 mmol dm^{-3}) (a) with no applied bias potential and (b) at an applied bias potential of 0.2 V *vs*. SCE. (B) Photocurrent action spectra of OTE/SnO_2/(**H-H_2P-COO-TiO_2**)$_n$ ([**H_2P**] = 0.025 mmol dm^{-3}) (a) with no applied bias potential and (b) at an applied bias potential of 0.2 V *vs*. SCE. (C) Photocurrent action spectra of OTE/SnO_2/(**H_2P-4COO-TiO_2**)$_n$ ([**H_2P**] = 0.025 mmol dm^{-3}) (a) with no applied bias potential and (b) at an applied bias potential of 0.2 V *vs*. SCE. electrolyte: 0.5 mol dm^{-3} NaI and 0.01 mol dm^{-3} I_2 in acetonitrile.

Figure 7. (A) Photocurrent action spectra of OTE/SnO_2/(**Ar-H_2P-COO-TiO_2**+C_{60})$_n$ ([**H_2P**] = 0.025 mmol dm^{-3}, [C_{60}] = 0.13 mmol dm^{-3}) (a) with no applied bias potential and (b) at an applied bias potential of 0.2 V *vs*. SCE. (B) Photocurrent action spectra of OTE/SnO_2/(**H-H_2P-COO-TiO_2**+C_{60})$_n$ ([**H_2P**] = 0.025 mmol dm^{-3}, [C_{60}] = 0.13 mmol dm^{-3}) (a) with no applied bias potential and (b) at an applied bias potential of 0.2 V *vs*. SCE. (c) Sum of two individual IPCE values of OTE/SnO_2/(**H-H_2P-COO-TiO_2**)$_n$ (spectrum b in Figure 6B) and OTE/SnO_2/(C_{60})$_n$ (spectrum b in Figure 7D) at an applied bias potential of 0.2 V *vs*. SCE. (C) Photocurrent action spectra of OTE/SnO_2/(**H_2P-4COO-TiO_2**+C_{60})$_n$ ([**H_2P**] = 0.025 mmol dm^{-3}, [C_{60}] = 0.13 mmol dm^{-3}) (a) with no applied bias potential and (b) at an applied bias potential of 0.2 V *vs*. SCE. (D) Photocurrent action spectra of OTE/SnO_2/(C_{60})$_n$ ([C_{60}] = 0.13 mmol dm^{-3}) (a) with no applied bias potential and (b) at an applied bias potential of 0.2 V *vs*. SCE. electrolyte: 0.5 mol dm^{-3} NaI and 0.01 mol dm^{-3} I_2 in acetonitrile.

Figure 8. Power characteristics of (a) OTE/SnO_2/(**H-H_2P-COO-TiO_2**+C_{60})$_n$ ([**H_2P**] = 0.025 mmol dm^{-3}, [C_{60}] = 0.13 mmol dm^{-3}) and (b) OTE/SnO_2/(**H-H_2P-COO-TiO_2**)$_n$ ([**H_2P**] = 0.025 mmol dm^{-3}) under white light illumination (λ> 400 nm); electrolyte: 0.5 mol dm^{-3} NaI and 0.01 mol dm^{-3} I_2 in acetonitrile; input power: 6.8 mW cm^{-2}.

Figure 1

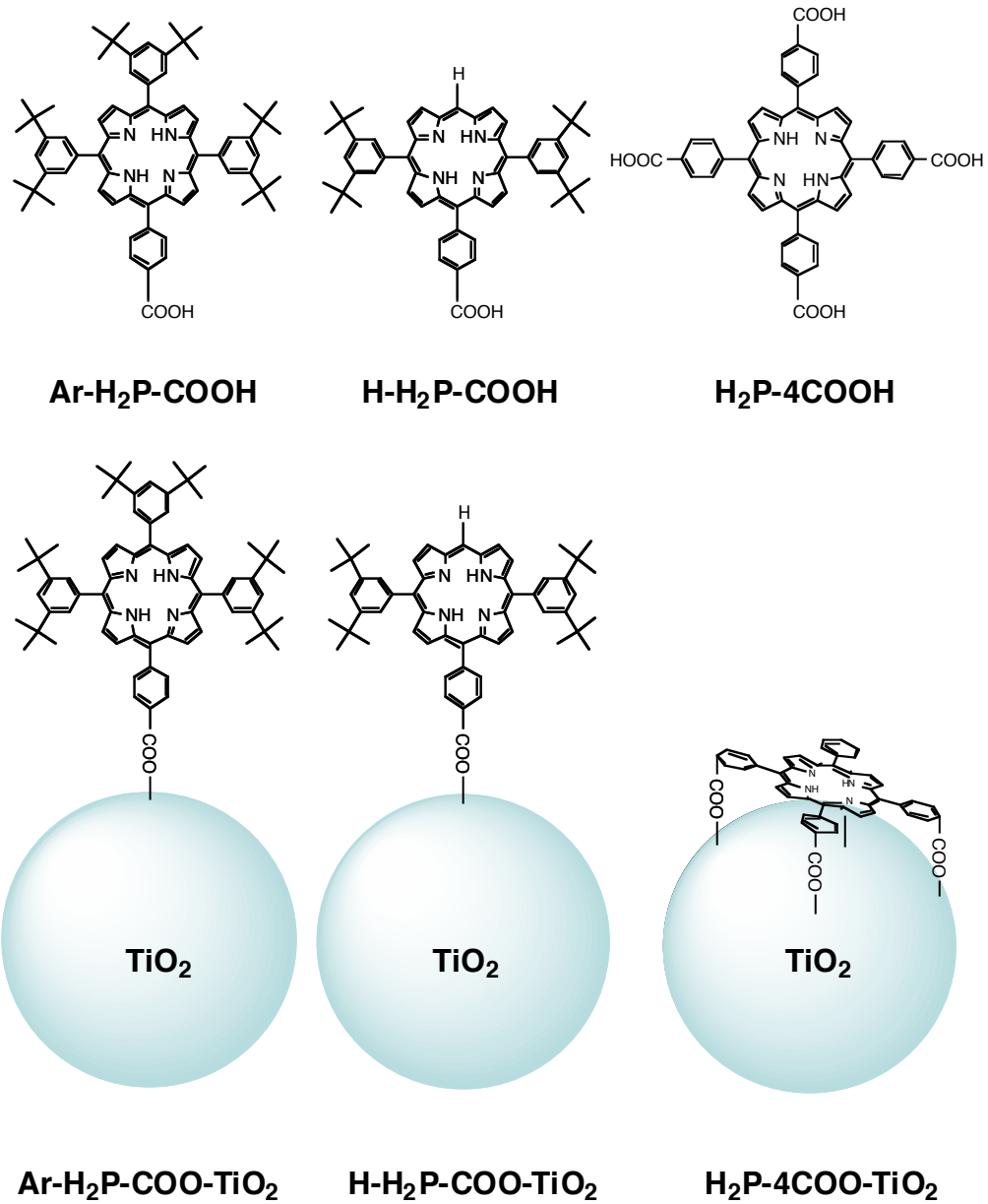
COOH
H
HOOC
COOH
N
HN
NH
TiO2
Ar-H2P-COOH
H-H2P-COOH
H2P-4COOH
Ar-H2P-COO-TiO2
H-H2P-COO-TiO2
H2P-4COO-TiO2

Figure 2

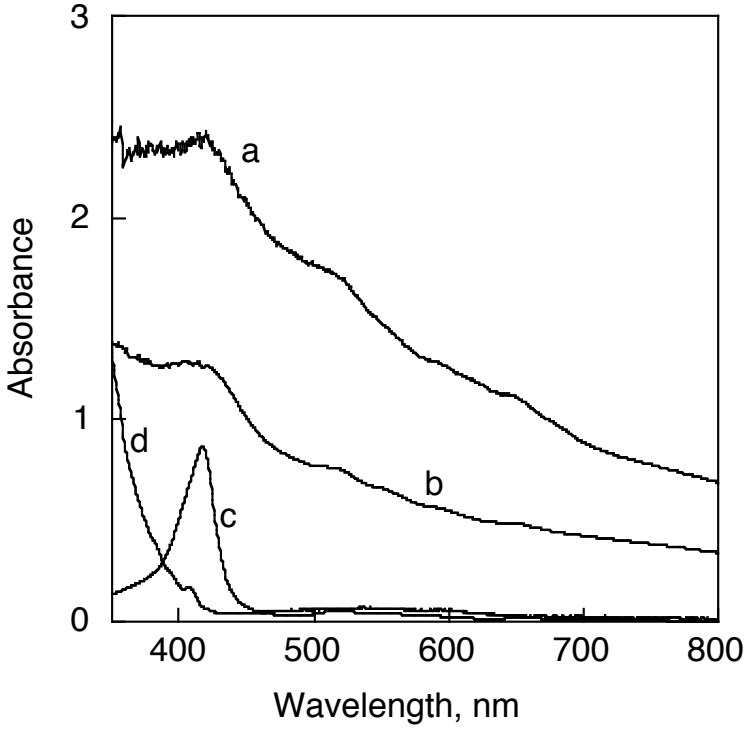

Figure 3

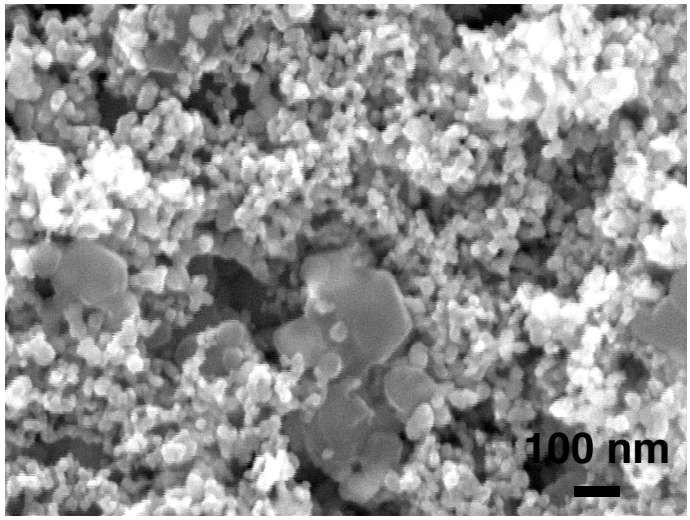

Figure 4

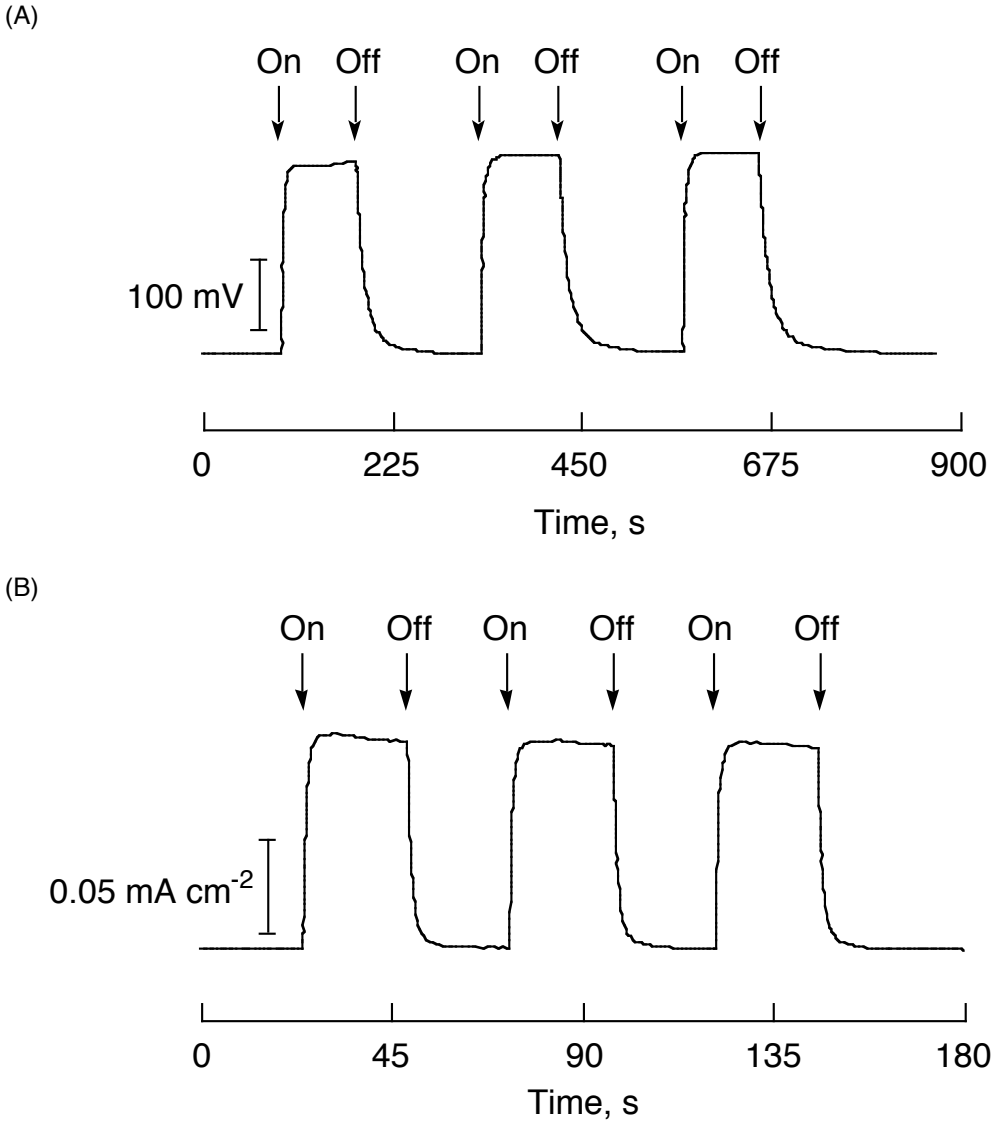
(A)
On
Off
On
Off
On
Off
100 mV
0
225
450
675
900
Time, s
(B)
On
Off
On
Off
On
Off
0.05 mA cm-2
0
45
90
135
180
Time, s

Figure 5

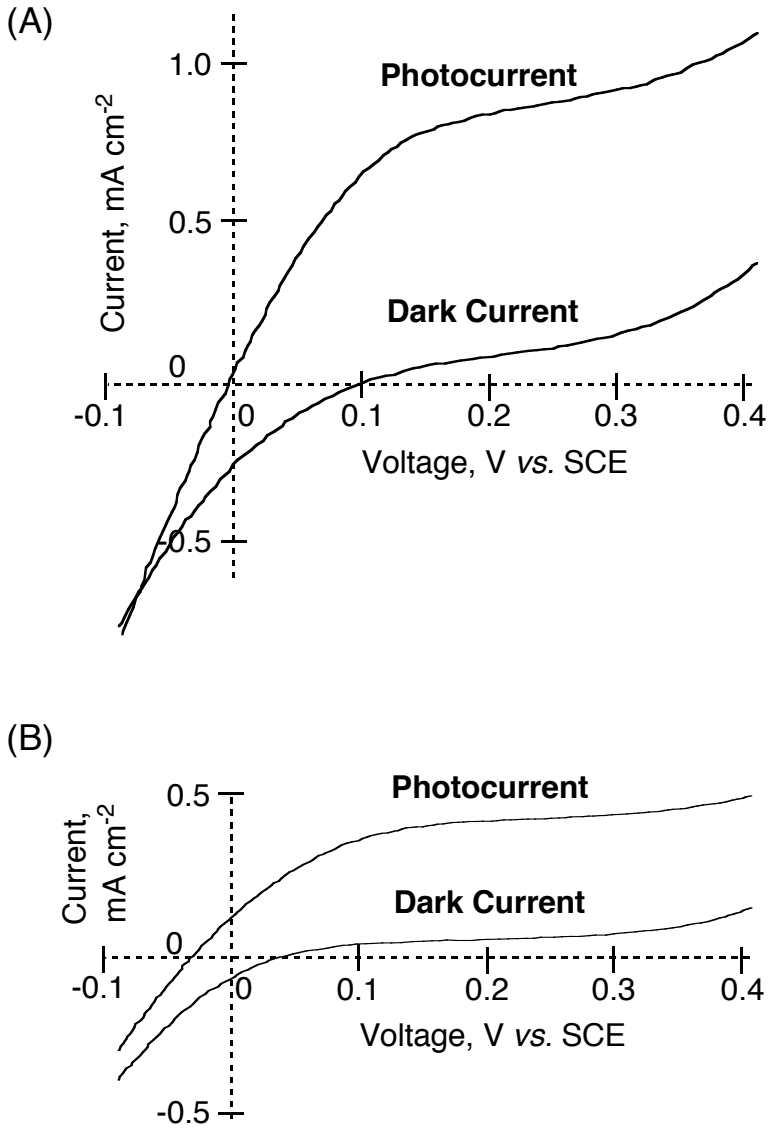
(A)
1.0
0.5
0
-0.5
Current, mA cm-2
Photocurrent
Dark Current
-0.1
0
0.1
0.2
0.3
0.4
Voltage, V vs. SCE
(B)
0.5
0
-0.5
Current, mA cm-2
Photocurrent
Dark Current
-0.1
0
0.1
0.2
0.3
0.4
Voltage, V vs. SCE

Figure 6

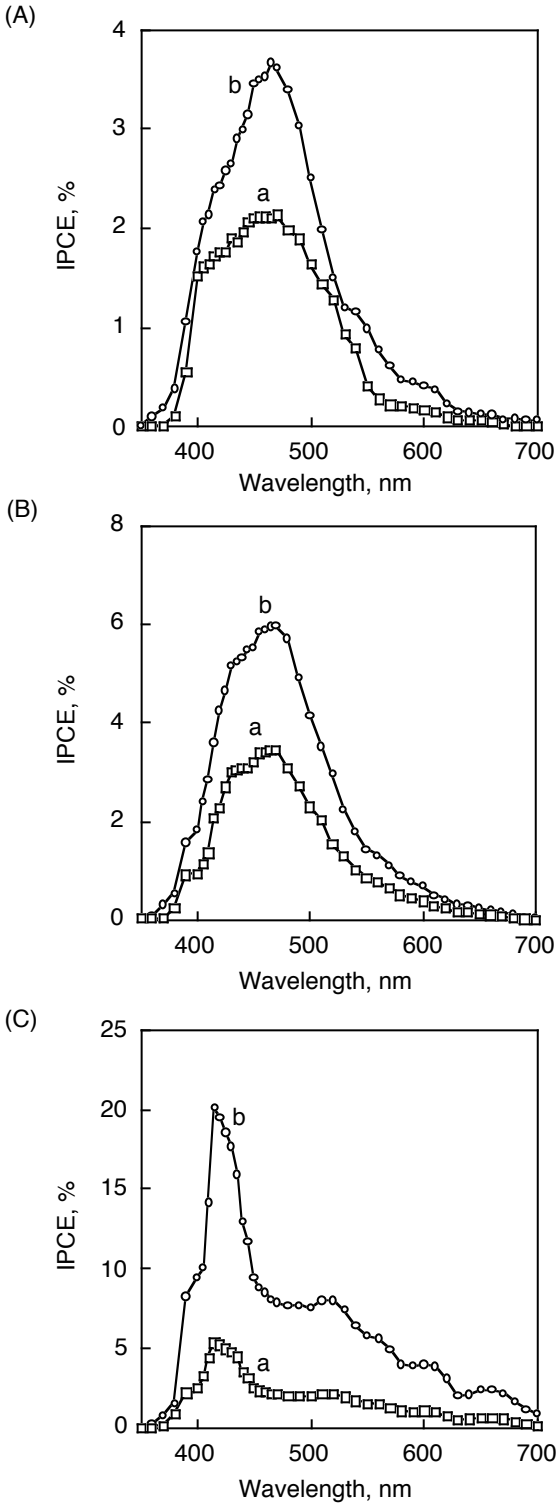
(A)
IPCE, %
Wavelength, nm
b
a
(B)
IPCE, %
Wavelength, nm
b
a
(C)
IPCE, %
Wavelength, nm
b
a

Figure 7

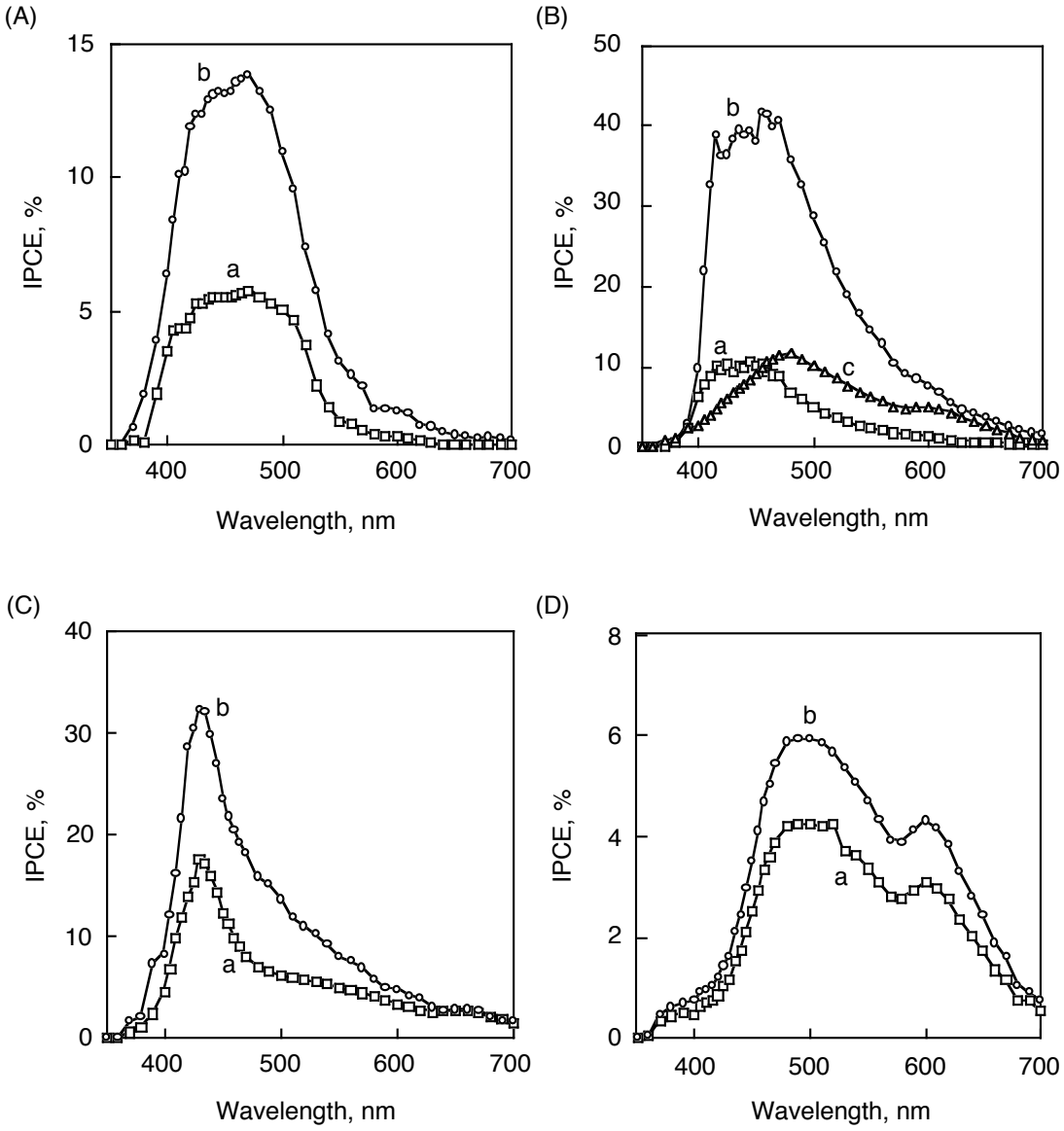
(A)
IPCE, %
Wavelength, nm
a
b
(B)
IPCE, %
Wavelength, nm
a
b
c
(C)
IPCE, %
Wavelength, nm
a
b
(D)
IPCE, %
Wavelength, nm
a
b

Figure 8

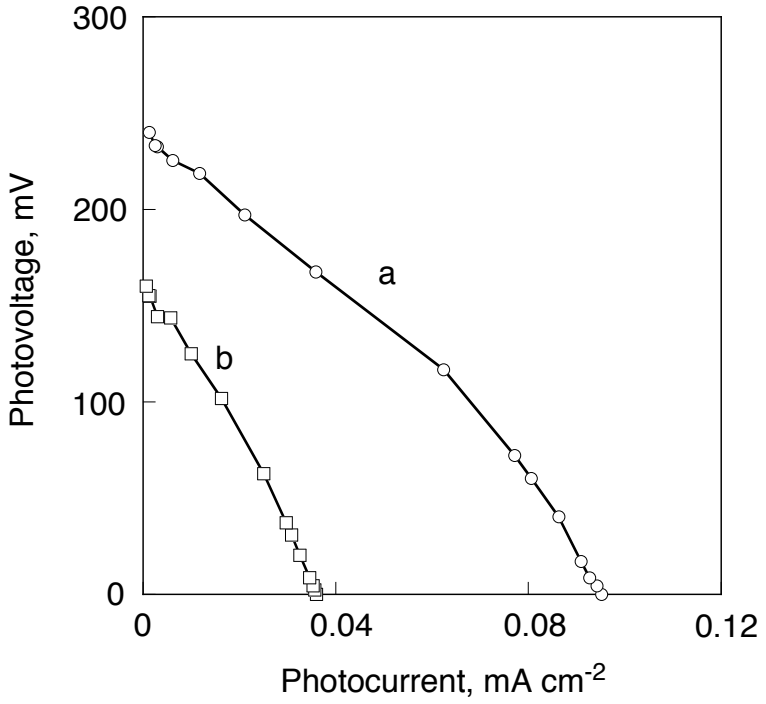
300
200
100
0
Photovoltage, mV
a
b
0
0.04
0.08
0.12
Photocurrent, mA cm-2